Astron. Astrophys. 256, 159–165 (1992)

ASTRONOMY AND ASTROPHYSICS

Atmospheric model and dynamical state of the atmosphere of the supergiant Eta Leonis (A0Ib)

A. Lobel*[1], L. Achmad[1], C. de Jager[1,2], and H. Nieuwenhuijzen[1,2]

[1] SRON Laboratory for Space Research, Sorbonnelaan 2, NL-3584 CA Utrecht, The Netherlands
[2] Astronomical Institute, Princetonplein 5, NL-3584 CC Utrecht, The Netherlands

Received August 2, accepted September 28, 1991

Abstract. We redetermined the atmospheric model parameters of η Leo (A0Ib) on the basis of a set of equivalent width data of 47 FeI and 71 FeII lines, determined previously by B. Wolf 1971. The procedure followed is an iterative one, involving the determination of the depth variation of microturbulence. We find: $T_{\rm eff}$ = 10200 K $\pm$ 370; log g = 1.9 [cm s^{-1}] $\pm$ 0.4 and $\triangle$log$Z$ (= logarithmic abundances compared to the solar values) = 0.14 $\pm$ 0.10 for Fe. A further result is that the line of sight microturbulence velocity component ζ_μ hardly varies with depth and equals 5.4 km s^{-1} $\pm$0.7, hence the motion field, which consists of isothermal shock waves, obeys the 'limiting shockstrength regime'. The observationally determined shock strenght is $M_{\rm s}^{\rm obs}$ = 2.3.

Key words: stars:atmospheres of – stars:supergiant – turbulence – shock waves – stars:individual η Leo

1. Introduction

In the framework of a study of the motion fields in the atmospheres of super- and hypergiants close to the Humphreys-Davidson limit (Humphreys, R. M. & Davidson, K. 1979), we have re-investigated the microturbulent atmospheric motion field of the supergiant η Leo (A0Ib). This star has previously been investigated by Wolf 1971, with the following main results:

Effective temperature	$T_{\rm eff}$ = 10400 K $\pm$ 300;
Gravitational acceleration	log g = 2.05 cm s^{-1} $\pm$ 0.20;
Average abundance	$\triangle$log$Z$ $\approx$ 0.25;
Microturbulence	from 2 km s^{-1} at $\bar{\tau}$ = 1.3 to 10 km s^{-1} in the outermost layers;
Macroscopic motion	ξ = 15 km s^{-1};
Luminosity	L/L$_\odot$ $\approx$ 15000;
Radius	R/R$_\odot$ $\approx$ 40;
Mass	M/M$_\odot$ $\approx$ 9.

We thought that it might be useful to re-investigate Wolf's observational material (from which we used the equivalent width data of 320 spectral lines in the wavelenght interval 3150Å < λ < 6565Å) for two reasons. First, we wish to study the depth dependence of the line-of-sight microturbulence velocity component, by making use of a new method (Achmad et al. 1991) for determining the average optical depth to which the observed microturbulence refers. Secondly, it is known that in supergiant atmospheres the observed microturbulence is due to a field of shock waves (De Jager et al. 1991). We wish to study the properties of this shock wave field, notably the shock strength and its variation with depth. In this paper we follow the same line of research as in a parallel study on α Car (Achmad et al. 1991a). The description of this study can therefore be brief.

*On leave from Astrophysical Institute, Vrije Universiteit Brussel, Pleinlaan 2, B-1050 Brussels, Belgium

2. Previous observations and model atmospheres

2.1. Data on the star and previous observations

The main observed properties and other general data on η Leo are given in Table 1.

Table 1. Data on η Leo

names	η Leo, HD 87737, HR 3975
spectral type	A0Ib
distance	0.56[2], 0.5[4], 1.25[5] kpc
M_v	−5.2[8], −5.3[1,11]
M_b	−5.4[8], −5.7[1,11]
m_v	3.53[2,6], 3.48[5,7,8], 3.31[9], 3.508[12]
Mass	9[1,11], 10[8] M$_\odot$
Radius	40.5[2], 40[1,3], 39[8], 41[11] R$_\odot$
$v$sini	18[4], 20[8,11], 24[10] km s^{-1}
$\dot{M}$	4. 7 10^{-8} M$_\odot$/yr [11]
v_∞	300[2], 293[3], 316[8], 283[11] km s^{-1}

[1]Wolf 1971; [2]Barlow 1977; [3]Lamers 1978; [4]Stokes 1978; [5]Cash 1979; [6]Clarck 1979; [7]Kondo 1979; [8]Praderie 1980; [9]Fernie 1983; [10]Zorec 1983; [11]Talavera 1987; [12]Rufener 1988

2.2. Previous model atmospheres

Several authors have already derived and published data on the effective temperature ($T_{\rm eff}$), gravity acceleration (log g), microturbulence (ζ_μ) and iron abundance ([Fe/H]) for η Leo. These data are collected in Table 2.

Table 2. List of previous model parameters of η Leo, derived by several authors.

Author, year	$T_{\rm eff}$ (K)	log g (cm s^{-2})	ζ_μ (km s^{-1})	[Fe/H] (solar)
Przybylski, 1969	$\sim$ 9330	$\sim$ 1.5	4. 6 (FeII)	- 0. 3
Kopylov, 1970	10350	2. 17	-	-
Wolf, 1970	10400	2. 05	2 to 10	0. 18
Morel, 1976	-	-	-	-0. 10
Boesgaard, 1978	9400	2. 0	-	-
Underhill, 1982	9400	-	-	-
Talavera, 1987	9730	-	-	-

3. The photospheric model parameters

The aim of this analysis is to investigate the depth dependence of the microturbulence, for which we know that it is sensitive to the model atmosphere ($T_{\rm eff}$, log g) adopted. We selected equivalent width data from 320 neutral and singly ionized lines, coming from various elements. Table 3 lists the number of original lines of each element used in the analysis.

3.1. Analysis using various elements

A full description of the method to determine directly $T_{\rm eff}$, log g, ζ_μ and the abundance from a given set of observed equivalent widths can be found in Achmad et al. 1991a. This *method of linearization* is based on the requirement that the calculated equivalent widths of all lines, for a choosen set of stellar parameters, should be roughly equal to their observed equivalent widths. Assuming that the calculated equivalent widths differ not more than 50% from the observed values, we selected 200 lines out of the original set of 320 observed spectral lines. It seems allowed to delete observations with larger error because such large errors are not expected to be produced by the numerics of the method of analysis, and they must be due to not-notified line blending or to grossly inaccurate gf -values. These values were taken from Wolf's paper. An extended list of references to the sources of the oscillator strengths of various elements can be found therein.

Starting from Wolf's parameters for the atmosphere $T_{\rm eff}$ = 10400 K, log g = 2.05 cm s^{-2}, choosing ζ_μ = 3.5 km s^{-1} and assuming solar abundance (Ross & Aller 1976) for all elements, we derived improved values in successive approximations using Kurucz models (1979). After 4 iterations we conclude that the best model atmosphere for η Leo, using various elements is: $T_{\rm eff}$ = 10700 K $\pm$ 200; log g = 1.8 cm s^{-2} $\pm$ 0.15; ζ_μ = 5.3 km s^{-1} $\pm$ 0.4 and $\triangle \log Z = 0.23 \pm 0.12$. The error ranges result from a least square method over all calculated lines. We note that the microturbulence velocity found here is an average value over the depth of the atmosphere.

3.2. Depth dependence of ζ_μ for various elements

Having found the photospheric parameters of η Leo we proceede to a determination of the depth dependence of the microturbulence velocity component.

For each spectral line the *average depth of formation* was determined according to the method of Achmad et al. 1991b, together with its ζ_μ-value, by varying the calculated equivalent width until it equals the observed value, keeping the other parameters constant. Figure 1 shows a plot of their ζ_μ-values against the Rosseland mean optical depth $\tau_{\rm Ross}$ for the model with $T_{\rm eff}$ = 10700 K and log g = 1.8 cm s^{-2}. We also plot the error bars in the derived ζ_μ-values, assuming an average error of 10% in the observations of the equivalent widths. From this graph we find that there is no significant depth-dependence of the microturbulence velocity component.

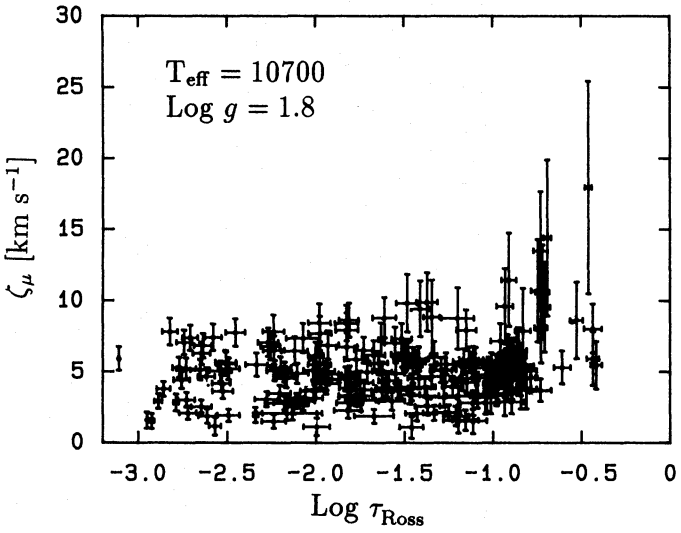

Fig. 1. Microturbulence velocity component ζ_μ against Rosseland mean optical depth for the model with $T_{\rm eff}$ = 10700 K and log g = 1.8 cm s^{-2}

Wolf 1971 adopted a depth-dependent microturbulence velocity component $\zeta_\mu(\bar{\tau})$ that increases outwards. However, in Sect. 3.5 we discuss the assumptions on which this result is based, and why this doesn't lead to the constant microturbulence that we find.

In Fig. 2 we plot the averaged depth-dependence of the microturbulence for the most important elements (the elements with the largest number of lines which fitted to better than 50% with the observations in the iteration procedure). This graph was produced using a smoothing function and taking into account the weights of the various values as determined by the error on each line. Table 3 gives a list of the mean values of microturbulence (by integration throughout the atmosphere) $< \zeta_\mu >$ for each element, together with the number of lines selected by the iteration procedure. The dotted line in Fig. 2 indicates the averaged value of all elements against the Rosseland mean optical depth. Throughout the whole atmosphere it has a mean value of 4.4 km s^{-1}. Notice that this value is not within the error range of 5.3 km s^{-1} $\pm$ 0.4 found by iteration, but it is still comparable.

From this graph we find that the calculated equivalent widths of singly ionized Vanadium are systematically too high when using this model. This is because we have to lower the model-microturbulence $\zeta_\mu^{\rm model}$ = 5.3 km s^{-1} until the calculated and observed equivalent widths are nearly equal. It is an indication that the abundance of VII in η Leo is lower than the $\triangle \log Z = 0.23$ derived for this model. At a certain optical depth we expect one and the same ζ_μ-value for all elements. Moreover, the difference between $< \zeta_\mu >_{\rm FeI}$ and $< \zeta_\mu >_{\rm FeII}$ is another indication that our model is not determined accurately enough. Inaccuracies can result from the different abundance corrections for the various elements in the method of linearization. Because of the larger number of parameters, the convergence in the iteration will slow

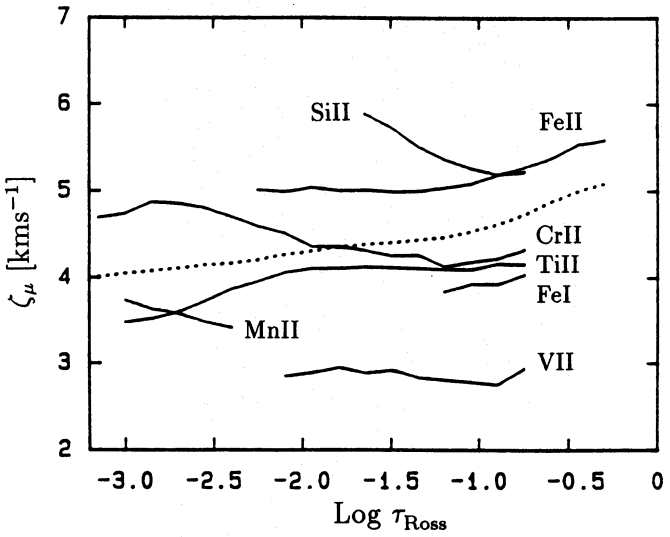

Fig. 2. Averaged microturbulence velocity throughout the atmosphere for the most important elements in the analysis. The dotted line indicates the averaged values for all elements together

Table 3. Number of original lines used in the analysis and the number of selected lines by the iteration procedure where the mean microturbulence velocity component $< \zeta_\mu >$ [km s^{-1}] is calculated with.

element	# original lines	# selected lines	$< \zeta_\mu >$
CI	1	0	-
OI	3	0	-
MgI	3	0	-
MgII	7	1	-
AlI	2	1	-
SiII	9	7	5. 5
CaII	2	1	-
ScII	5	3	-
TiII	84	62	4. 0
VII	12	8	2. 8
CrII	62	49	4. 8
MnII	7	7	3. 6
FeI	47	4	3. 9
FeII	71	55	5. 2
CoII	1	0	-
NiII	4	2	-
total	320	200	4. 4

down. This is because incertainties in one parameter give errors in the values of the other parameters.

3.3. *Analysis using only iron lines*

In this section we will repeat our analysis, but now only using the original set of 118 (47 FeI and 71 FeII) observed iron lines. Hence, we try to avoid inaccuracies as discussed in the previous section.

Starting from the initial values: $T_{\rm eff}$ = 10000 K, log g = 2.0 cm s^{-2}, ζ_μ = 6.0 km s^{-1} and $\triangle \log Z$ = 0.0 (solar abundance), we find after 3 iterations *the best iron-model* parameters: $T_{\rm eff}$ = 10300 K$\pm$370, log g = 1.9$\pm$0.4, ζ_μ = 6.6$\pm$0.7 and $\triangle \log Z_{\rm Fe}$ = 0.10$\pm$0.13. These values are in good agreement with those from the previous model derived using various elements (except that $\zeta_\mu = 6.6 \pm 0.7$ is not within the error range derived with the previous model where $\zeta_\mu = 5.3 \pm 0.4$, but they remain comparable).

This leads to the important conclusion that it is reasonable to derive the optimal model parameters using only one species and hence improving the reliability of method of the approximation. We notice this because in general an extended set of equivalent width data of various species is not available.

3.4. *Depth dependence of ζ_μ for the iron lines*

In Fig. 3 the depth dependence of the microturbulence velocity component is plotted for 63 retained Fe lines. Figure 4 shows the averaged value of the ζ_μ -component throughout the atmosphere for neutral and singly ionized lines. Still there remains a difference in the mean values $< \zeta_\mu >_{\rm FeI}$ = 7.3 km s^{-1} and $< \zeta_\mu >_{\rm FeII}$ = 6.1 km s^{-1}. Notice the good agreement of these values with the model value of 6.6 km s^{-1} $\pm$0.7, derived from the iteration method.

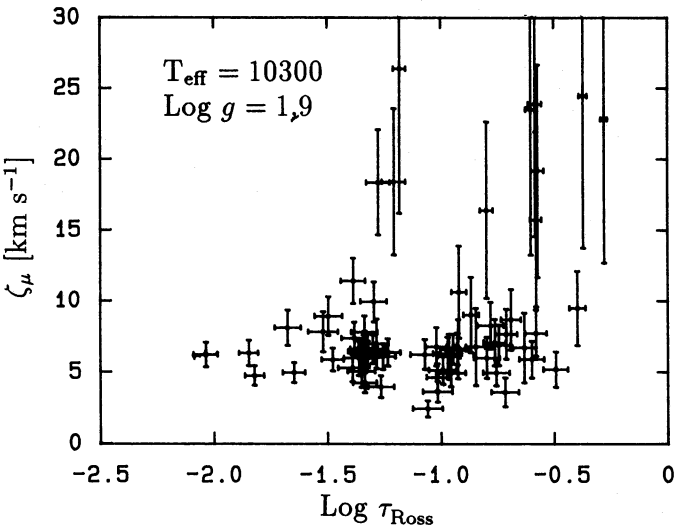

Fig. 3. Depth dependence of the microturbulence velocity component for the iron lines, using the model with $T_{\rm eff}$ = 10300 K and log g = 1.9 cm s^{-2}

The difference between both values disappears when decreasing the $T_{\rm eff}$ of the iron-model with only 100 K, as is shown in Fig. 5. The calculated individual microturbulence for each line is derived for the Kurucz model with this lowered $T_{\rm eff}$ = 10200 K. Now, 78 lines (19 FeI and 59 FeII) are retained instead of 63, which indicates that the model parameters improved.

Table 4 gives a list of the lines shown in Fig. 5. The solid line in Fig 5 represents the averaged microturtulence through the atmosphere for FeII. It is calculated taking into account the weights of the various individual microturbulence values as determined by their errors. For the clarity of this figure, we dropped the errorbars.

Since the ζ_μ -value at a certain optical depth will be influenced by the neighbouring layers, a smoothing function is used to find the mean ζ_μ -function (for a detailed discussion we refer to Achmad et al. 1991a). The tiny dashed line in Fig. 5 gives the averaged microturbulence for FeI. Finally, when integrating these functions over the whole atmosphere, $< \zeta_\mu >_{\rm FeI}$ obtains a value of 5. 38 km s^{-1} and $< \zeta_\mu >_{\rm FeII}$ of 5. 35 kms^{-1}. We notice that

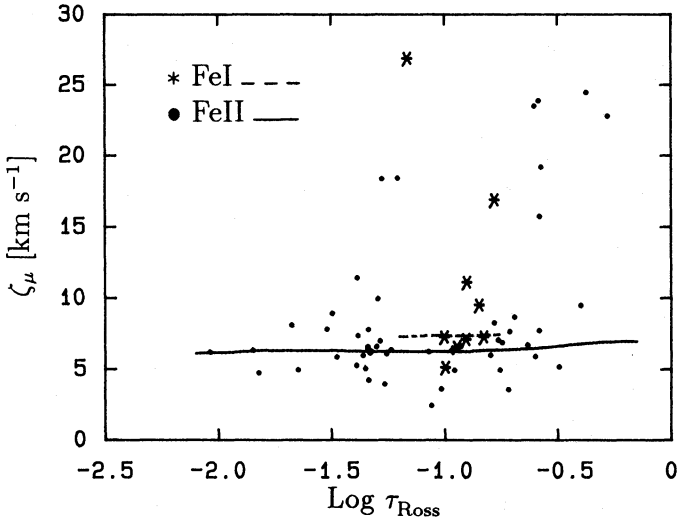

Fig. 4. Averaged microturbulence velocity component for FeI and FeII, using the model with T_{eff} = 10300 K and log g = 1.9 cm s^{-2}

these values are almost exactly the same as the value of 5. 8 km s^{-1} found by Wolf for $\bar{\tau}$ = 0.1, where the bulk of lines is formed. Notice also from Table 4 that all ranges of equivalent widths (weak, medium and strong) are covered. Hence, a reliable mean value of the microturbulence velocity over the atmosphere is derived.

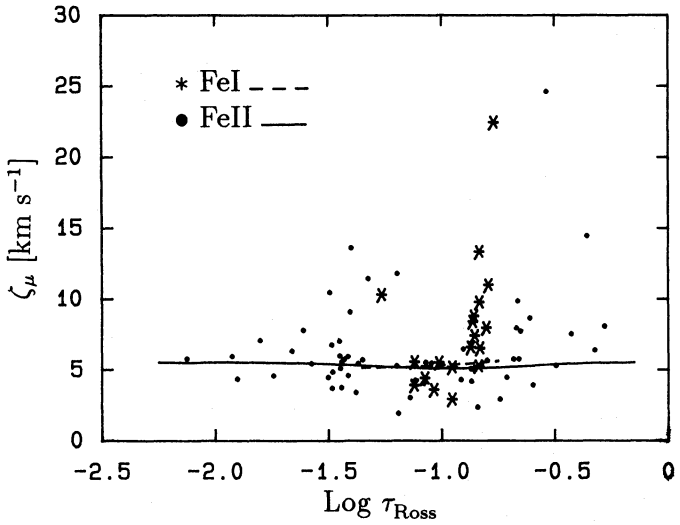

Fig. 5. Averaged microturbulence velocity component for FeI and FeII, using the model with T_{eff} = 10200 K and log g = 1.9 cm s^{-2}

3.5. Adjustment of T_{eff} and redetermination of the iron abundance

When applying this method to remove the difference in microturbulence between FeI and FeII, we find a new T_{eff} = 10200 K ±370 and a new $<\zeta_\mu>_{Fe}$ = 5.4 km s^{-1} ± 0.7. However, since we know that changes in one parameter will affect the values of the other parameters in the iteration method, we will have to redetermine the iron abundance.

This analysis was done with a constant log g -value while adapting the effective temperature T_{eff}. We note that it is also

Table 4. Microturbulence velocity with error and abundance values of neutral and ionized iron as calculated from the individual lines where the final model parameters were set with

Mult. Nr.	λ(Å)	loggf	W_λ	ζ_μ	±ζ_μ	△log$Z$
FeI						
4	3859. 9	-0. 65	69. 2	5. 02	1. 29	0. 09
	3899. 7	-1. 35	21. 4	12. 89	5. 39	0. 16
5	3745. 6	-0. 73	47. 9	3. 10	0. 92	0. 00
20	3820. 4	0. 24	112. 1	5. 08	0. 97	0. 07
	3825. 9	0. 06	79. 5	3. 92	0. 83	0. 00
21	3727. 6	-0. 44	32. 4	2. 42	0. 87	-0. 01
	3743. 4	-0. 56	31. 6	6. 04	2. 04	0. 12
	3758. 2	-0. 17	70. 8	8. 31	2. 24	0. 17
	3763. 8	-0. 08	66. 1	4. 69	1. 26	0. 06
22	3813. 0	-0. 79	19. 7	4. 79	2. 30	0. 10
24	3570. 1	0. 25	50. 1	9. 82	2. 47	0. 24
41	4383. 5	-0. 06	55. 0	7. 90	2. 40	0. 16
	4404. 8	-0. 14	42. 7	6. 91	2. 16	0. 13
42	4271. 8	-0. 12	50. 1	9. 30	3. 09	0. 16
43	4045. 8	0. 43	79. 5	3. 40	0. 69	-0. 06
	4071. 7	-0. 10	50. 1	21 . 94	9. 52	0. 24
45	3815. 8	0. 16	69. 2	6. 11	1. 49	0. 12
	3827. 8	0. 05	60. 3	10. 51	3. 38	0. 18
	3841. 1	-0. 05	44. 7	7. 49	2. 45	0. 15
FeII						
1	3302. 9	-3. 61	100. 0	6. 34	0. 96	
	3303. 5	-3. 34	128. 9	7. 09	0. 99	
4	3503. 5	-3. 95	42. 7	11. 82	3. 41	0. 25
	3508. 2	-3. 81	39. 8	4. 57	1. 06	0. 07
5	3425. 6	-3. 51	93. 3	11. 48	2. 37	
14	3746. 6	-3. 96	50. 2	2. 35	0. 65	-0 . 08
	3783. 3	-3. 45	138. 9	6. 49	1. 08	0. 21
16	3507. 4	-3. 36	39. 8	3. 69	0. 84	-0. 05
	3416. 0	-2. 86	144. 6	13. 65	2. 29	
21	4119. 5	-4. 42	30. 9	24. 63	11. 44	0. 22
	4177. 7	-3. 73	97. 7	9. 87	2. 63	0. 25
27	4128. 7	-3. 83	74. 2	7. 73	1. 94	0. 17
	4233. 2	-2. 58	298. 2	9. 10	1. 20	
	4351. 8	-2. 58	240. 0	7. 02	0. 99	
	4416. 8	-2. 75	178. 0	5. 44	0. 77	0. 10
	4303. 2	-2 . 69	199. 5	5. 94	0. 89	0. 21
	4273. 3	-3. 54	93. 4	5. 66	1. 19	0. 10
	4173. 5	-2. 74	195. 0	5. 74	0. 86	0. 16
28	4122. 6	-3. 52	97. 7	5. 04	0. 95	0. 08
	4178. 9	-2. 43	195. 0	4. 57	0. 65	- 0. 11
	4296. 6	-3. 14	141. 1	5. 55	0. 84	0. 11
	4258. 2	-3. 52	93. 4	5. 30	1. 09	0. 10
32	4278. 1	-3. 94	52. 5	5. 78	1. 57	0. 11
	4314. 3	-3. 33	87. 1	3. 01	0. 55	-0. 16
	4413. 6	-4. 17	38. 9	8. 67	2. 82	0. 15
37	4472. 9	-3. 34	66. 1	1. 92	0. 52	-0. 25
	4491. 4	-2. 94	151. 2	5. 30	0. 77	0. 10
	4515. 3	-2. 63	190. 7	5. 57	0. 81	0. 13
	4520. 2	-2. 76	182. 0	5. 73	0. 85	0. 20
	4555. 9	-2. 60	204. 0	5. 00	0. 91	0. 24
	4582. 8	-3. 23	102. 3	4. 03	0. 72	-0. 03
	4629. 3	-2. 14	209. 0	4. 36	0. 63	
	4666. 8	-3. 47	83. 2	4. 29	0. 95	0. 03
38	4508. 3	-2. 46	204. 0	5. 4 4	0. 81	0. 15
	4522. 6	-2. 49	234. 2	6. 78	1. 07	

Table 4. (continued)

Mult. Nr.	λ(Å)	loggf	W_λ	ζ_μ	$\pm\zeta_\mu$	$\triangle$log$Z$
	4541. 5	-3. 13	132. 0	5. 48	0. 90	0. 13
	4549. 5	-2. 30	363. 3	10. 49	1. 28	
	4576. 3	-3. 10	132. 0	5. 20	0. 89	0. 10
	4620. 5	-3. 47	89. 1	5. 04	1. 06	0. 08
	4583. 8	-1. 98	275. 9	5. 94	0. 90	
43	4731. 4	-3. 16	109. 8	4. 24	0. 73	-0. 09
	4657. 0	-3. 79	61. 7	7. 97	2. 28	0. 18
44	4663. 7	-3. 99	33. 9	2. 90	1. 01	0. 02
74	6147. 7	-2. 34	120. 1	3. 38	0. 64	-0. 14
	6247. 6	-2. 48	102. 0	3. 75	0. 65	-0. 16
91	3436. 1	-2. 11	61. 7	4. 85	0. 90	0. 07
	3297. 9	-2. 07	64. 6	4. 46	0. 81	0. 01
112	3614. 9	-2. 07	55. 0	5 . 12	0. 11	0. 09
114	3493. 5	-0. 98	141. 1	5. 78	0. 88	
	3468. 7	-1. 57	117. 5	7. 78	1. 19	
127	3845. 2	-2. 47	89. 1	4. 45	0. 86	0. 04
	3865. 0	-2. 98	51. 3	7. 56	2. 18	0. 16
130	3781. 5	-3. 1 7	39. 8	14. 48	5. 77	0. 20
172	4048. 8	-2. 17	69. 2	5. 30	1. 09	0. 12
173	3935. 9	-1. 61	109. 8	4. 19	0. 72	-0. 04
186	4635. 3	-1. 67	102. 2	5. 76	1. 11	0. 14
190	3938. 9	-1. 82	72. 5	3. 92	0. 95	-0. 00
191	3975. 0	-2. 44	32. 4	6. 40	2. 23	0. 12
219	4598. 5	-1. 51	31. 6	8. 09	2. 67	0. 17

possible to change the log g -value keeping $T_{\rm eff}$ constant, in order to adjust the mean microturbulence $<\zeta_\mu>$ of FeI and FeII, but we did not follow that course.

Assuming a constant $<\zeta_\mu>_{\rm Fe}$-value of 5.4 km s^{-1} in the region of line formation where the final model was constructed with (hence $-1.5 < \log\tau_{\rm Ross} < -0.5$ because of FeI), we calculate $\triangle \log Z$ for each Fe line by varying the metallic model abundance difference of 0.19 until the calculated and observed equivalent widths of the selected lines in this region are equal. In Table 4 we present a list of the calculated individual abundances (compared to the solar abundance) of the 19 selected FeI and 47 FeII lines in this range of optical depths. We omitted the abundance-values of lines originating outside this range. Remark that by changing $\triangle \log Z$ deduced from each line, its 'average depth of formation' will change also. In Fig. 6 we plot the abundances of Table 4 against the optical depth. The errors are found by assuming an average error of 10% in the observed equivalent widths. When calculating the mean value, we find that for the 19 selected FeI lines in this region: $<\triangle\log Z>_{\rm FeI} = 0.11 \pm 0.06$,and by using the 47 selected FeII lines:$<\triangle\log Z>_{\rm FeII} = 0.09 \pm 0.10$. The mean value for all 66 Fe-lines together in this region of Rosseland mean optical depth is $<\triangle\log Z>_{\rm Fe} = 0.10 \pm 0.09$.

Summarized, we derive for the final model: $T_{\rm eff}$ = 10200 K$\pm$370, log g = 1.9 cm s^{-2} $\pm$ 0.4, $<\zeta_\mu>_{\rm Fe}$ = 5.4 km s^{-1} $\pm$ 0.7 and $<\triangle\log Z>_{\rm Fe} = 0.10 \pm 0.09$. Notice that the $T_{\rm eff}$ and log g -values are in good agreement with those derived by Wolf 1971. The iron abundance he found is $<\triangle\log Z>_{\rm Fe}$ = 0.18, which is also in good agreement with our value of 0.10. In addition, the mean microturbulence velocity $<\zeta_\mu>$ for FeII of 5.35 km s^{-1} $\pm$ 0.7 appears to correspond with the value found by Przybylski 1969 of 4. 6 km s^{-1}, using the vertical shift of the curve of growth (cfr. Table 2).

We return now to the discussion of the depth-dependence of the microturbulence. Wolf's method was also based on the determination of the 'mean depth of formation' of a line, which is associated to a ζ_μ -value. This value was found for the medium-strong and strong FeII and TiII lines by interpolation until the calculated equivalent width agreed with the observed value. The abundances for this calculation were taken from the weak lines using ζ_μ= 2.25 km s^{-1}. This assumption resulted from the systematic abundance differences that were found within a single multiplet when calculating with a constant microturbulence value of 2.25 km s^{-1}. The strong lines (which originate in a geometrically higher layer) can give abundance differences of one to two powers of 10 compared to the weak lines.

Using our final model with $T_{\rm eff}$=10200 K, log g=1. 9 and assuming a constant ζ_μ -value of 2. 25 km s^{-1}, we could reproduce this effect with our code. Hence, an abundance increasing with decreasing depth is indeed derived,which is basically a result of the dependence of the derived abundances on the line strength. However, when using the constant ζ_μ -value of 5. 4 km s^{-1}, derived from our analysis,we find that this tendency of increasing abundance in the outer layers and the abundance differences between the weak and strong lines within a multiplet, dissapear almost completely. Therefore, the need for a depth-variation of the microturbulence velocity dissapears, with the exception of the region with log $\tau_{\rm Ross}$ < -3 where a slight difference of 0. 4 from the average $\triangle\log Z$ -value of 0. 2 remains.

Another assumption that Wolf used to adopt an atmospheric model with increasing ζ_μ (up to 10 km s^{-1}) in the outer layers, is the higher abundances for the FeII, TiII and CrII lines on the short wavelenght side(which originate in a geometrically higher layer) of the Balmer jump (λ < 3647 Å) compared to those on the long wavelenght side. We selected for each element 2 multiplets formed before and after the Balmer jump, and calculated the $\triangle\log Z$ of each line using a constant ζ_μ=2.25 km s^{-1}. Here, we also found non-negligible abundance differences between the multiplets of the same element. However, when recalculating with ζ_μ=5. 4 km s^{-1} these differences become insignificant.

From our analysis we conclude that it is not strictly necessary to adopt an increasing microturbulence with decreasing depth in the atmospheric model of the supergiant η Leo. Using a constant value of 5. 4 km s^{-1} throughout the atmosphere, the dependence of the abundance on the line strength can adequately be removed. We note that from this method a constant microturbulence was also found in the supergiant α Car (F0Ib) (Achmad et al. 1991a) for equivalent width data from 694 FeI and FeII lines, probably the largest dataset ever used for this kind of investigation.

4. Properties of the shock wave field in η Leo

De Jager et al. 1991 found that the observed microturbulence in supergiant atmospheres is due to a field of shock waves. Cuntz & Ulmschneider 1988 found that under certain simplified conditions the amplitude of these waves remains constant(instead of increasing with decreasing density) when moving outwards, as a result of the dissipation of shock energy. Hence, it is believed that this observed constancy of ζ_μ with depth can be explained by assuming an atmosphere which obeys the 'limiting shock strength regime'.

The diagnostic diagram of the motion field at Rosseland mean optical depth $\tau_{\rm Ross}$ = 0.03 is shown in Fig. 7 (cfr. de

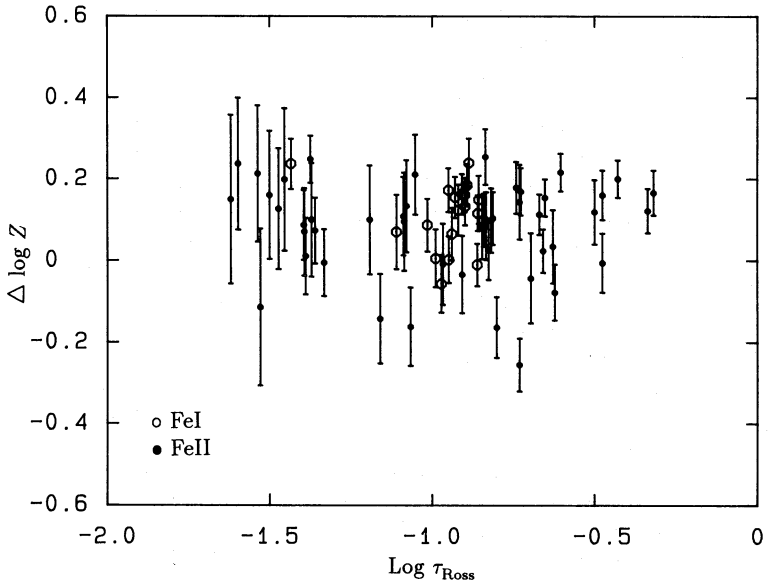

Fig. 6 Individual abundance and error (compared to the solar abundance) for FeI (open circles) and FeII (filled circles) in the region of optical depths where the final model was set with

Jager et al. 1991). From this graph we read that the observed microturbulence velocities are due to isothermal waves, for which the (isothermal) velocity of sound is $s = \sqrt{P/\rho} \approx 9.76\ 10^5$ cm s^{-1}. From Eqs. (54) and (61) of de Jager et al. 1991, we find that the longest wavelenght L_1 of the observed spectrum of shock waves has a value of $1.20\ 10^{10}$ cm, and the scale height $H \approx 8.42\ 10^{10}$ cm. Hence, $L_1/H \approx 7.02$. The average period of the waves $P = \frac{<L>}{s} \approx 4.86\ 10^4$ s, where the average wavelength $< L >= 0.75\ 10^{10}$ cm is calculated assuming a Kolmogoroff spectrum of turbulence, or $< L >= \frac{5}{8} L_1$.

Cuntz and Ulmschneider 1988 have derived a formula for the limiting shock strength $M_s^{\lim}$ in a stellar atmosphere. This value can be calculated from the average period P, the local speed of sound, effective acceleration g_{eff} of the atmospheric model and a constant $\gamma = 1.12$ (assumed to be the first adiabatic exponent, which we have calculated without radiation pressure here) at Rosseland mean optical depth $\tau_{\text{Ross}} = 0.03$, with a layer temperature $T = 8211$ K and gas pressure $P_g = 4.63$ dyn cm^{-2}. We find for $M_s^{\lim}$ a value of 2.11.

Nieuwenhuijzen & de Jager 1991 have developed an algorithm to calculate the 'observational' M_s^{obs} -value from the $< \zeta_\mu >$ -value that is derived from the analysis of observed equivalent width data. This method is based on the theoretical work of Gail et al. 1990. We find for M_s^{obs} a value of 2. 3,which is close to the value of the limiting shock strength.

5. Conclusions

We have redetermined the photospheric parameters of η Leo from a set of equivalent width data, measured by Wolf 1971. Our results for T_{eff}, log g, ζ_μ and abundance deviate only slightly from Wolf's. Our main result is, however, that the average microturbulence line of sight velocity component ζ_μ hardly varies with depth over the atmosphere. This means that the observed 'microturbulence' occurs in the limiting shockstrength regime.

Acknowledgements. We thank the Centre des Donneés in Strasbourg for supplying lists of literature on η Leo.

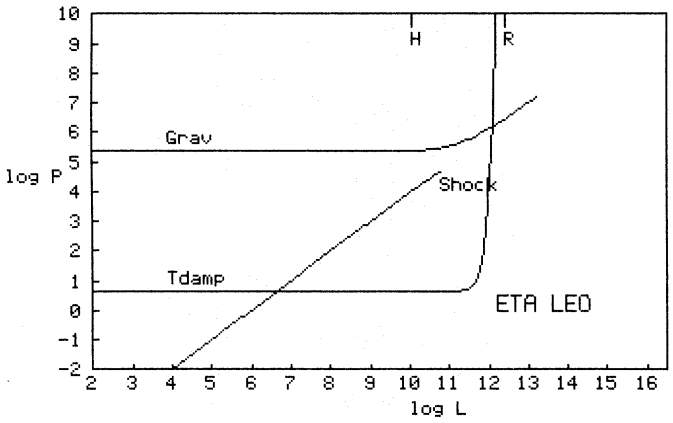

Fig. 7. Diagnostic diagram (period, wavelenght) for η Leo. On the line labeled *Shock*, pressure waves originate. Above the horizontal line T_{damp} these shocks are isothermal and below it they are adiabatic. The line *Grav* is the lower limit of the area where gravity waves are not evanescent. H is the scale height and R is the stellar radius

References

Achmad, L. , de Jager, C. , Nieuwenhuijzen, H. 1991a, 'Atmospheric model parameters and shock wave field of α Car, A&A, in press

Achmad, L. , de Jager, C. , Nieuwenhuijzen, H. 1991b, 'The depth of formation of spectral lines in stellar atmospheres', A&A, in press

Barlow, M. J. , Cohen, M. 1977, ApJ, 213, 737

Boer, B. , de Jager, C. , Nieuwenhuijzen, H. 1988, A&A, 195, 218

Boesgaard, A. , Heacox, W. 1978, ApJ, 226, 888

Carpay, J. , de Jager, C. , Nieuwenhuijzen, H. 1989, A&A, 216, 143

Cash, W. , Snow, T. P. , Charles, P. 1979, ApJ (L), 232, 111

Clarck, J. P. A. , McClure, R. D. 1979, PASP, 91, 507

Cuntz, M. , Ulmschneider, P. 1988, A&A, 193, 119

De Jager, C. , De Koter, A. , Carpay, J. , Nieuwenhuijzen, H. 1991, A&A, 244, 231

Fernie, J. D. 1983, ApJS, 52, 7
Gail, H. P. , Cuntz, M. , Ulmschneider, P. 1990, A&A, 234, 359
Kondo, Y. , de Jager, C. , Hoekstra, R. , Van der Hucht, K. A. , Kamperman, T. M. , Lamers, H. J. G. L. M. , Modisette, J. L. , Morgan, T. H. 1979, ApJ, 230, 526
Kopylov, I. 1970, Astrof. Isseledov, Leningrad, 2, 42
Kurucz, R. 1979, ApJ S, 40, 1
Lamers, H. J. G. L. M. , Stalio, R. , Kondo, Y. 1978 ApJ, 223, 207
Morel, M. , Bentolila, Cayrel, C. , Hauk, B. 1976, 'Abundance Effects in Classification', UIA Symposium No. 72, p. 223, Reidel,Dordrecht
Nieuwenhuijzen, H. , de Jager, C. 1991, 'The Shock Strenght in supergiant atmospheres', A&A (in preparation)
Praderie, F. , Talavera, A. , Lamers, H. J. G. L. M. 1980, A&A, 86, 271
Przybylski, A. 1969, MNRA S, 146, 71
Ross, J. F. , Aller, L. H. 1976, Sci, 191, 1223
Rufener, F. 1988, 'Catalogue of Stars measured in the Geneva Observatory Photometric system (fourth ed.)', Sauverny, Geneva Observatory Publications
Stokes, G. M. 1978, ApJS, 36, 115
Talavera, A. , Gomez de Castro, A. I. 1987, A&A, 181, 300
Underhill, A. , Doazan, V. 1982, 'B Stars With and Without Emission Lines', NASA SP-456
Wolf, B. 1971, A&A , 10, 383
Zorec, J. , Briot, D. , Divan, L. 1983, A&A, 126, 192

This article was processed by the author using Springer-Verlag LaTeX A&A style file 1990.